FORCED CONVECTION BOUNDARY LAYER MAGNETOHYDRODYNAMIC FLOW OF NANOFLUID OVER A PERMEABLE STRETCHING PLATE WITH VISCOUS DISSIPATION

by

Meisam HABIBI MATIN [a,b] ***and Pouyan JAHANGIRI*** [c*]

[a] Department of Mechanical Engineering, Kermanshah University of Technology, Kermanshah, Iran
[b] Young Researchers Club and Elites, Kermanshah Branch, Islamic Azad University, Kermanshah, Iran
[c] Department of Mechanical Engineering, University of British Columbia, Vancouver, Canada

Original scientific paper
DOI: 10.2298/TSCI120403049H

Forced convection boundary layer magnetohydrodynamic flow of a nanofluid over a permeable stretching plate is studied in this paper. The effects of suction--injection and viscous dissipation are taken into account. The nanofluid model includes Brownian motion and thermophoresis effects. The governing momentum, energy, and nanofluid solid volume fraction equations are solved numerically using an implicit finite difference scheme known as Keller-box method and the results are compared with available numerical data. The results for the dimensionless velocity, dimensionless temperature, dimensionless nanofluid solid volume fraction, reduced Nusselt and reduced Sherwood numbers are presented illustrating the effects of magnetic parameter, suction-injection parameter, Brownian motion parameter, thermophoresis parameter, Prandtl number, Eckert number and Lewis number.

Key words: *forced convection, nanofluid, permeable stretching plate, boundary layer, magnetohydrodynamics*

Introduction

The forced convection heat transfer over a permeable stretching plate has relevance in applications such as solar receivers exposed to wind currents, electronic devices cooled by fans, nuclear reactors cooled during emergency shutdown, heat exchanges placed in a low-velocity environment, extrusion processes, cooling of reactors, glass fiber production, and crystal growing [1-3]. During the last decade, nanofluid heat transfer problems have been given considerable attention by researchers. Conventional fluids, such as water, ethylene glycol mixture, and some types of oil have low heat transfer coefficients. The necessity for improving some physical fluid properties such as thermal conductivity and enhancing the heat transfer of pure fluids has led to the utilization of nanoparticles in the fluid. Choi [4] was the first who introduced the term "nanofluid". Choi *et al*. [5] concluded that the addition of one percent by volume of nanoparticles to pure fluids increases the thermal conductivity of the fluid by almost a factor of 2. Thus the performance of heat transfer systems can be significantly improved if regular fluids are replaced by nanofluids.

Buongiorno [6] was first one who formulated the nanofluid model taking into account the effects of Brownian motion and thermophores. In his work he indicated that although there are some elements that affect nanofluid flow such as inertia, Brownian diffusion,

* Corresponding author; e-mail: pj.autech@gmail.com

thermophoresis, diffusiophoresis, Magnus effect, fluid drainage and gravity, only Brownian diffusion and thermophoresis are important mechanisms in nanofluids.

Bachok *et al*. [7] numerically studied nanofluid forced convection boundary layer flow over a moving plate. They concluded that dual solutions exist when the plate and the free stream move in opposite directions. Khan and Pop [8] investigated the boundary layer flow of a nanofluid over a linearly stretching sheet. They found that the local Nusselt and Sherwood numbers decrease with Brownian and thermophoresis parameters as well as Prandtl and Lewis numbers. Hamad *et al*. [9] investigated the effect of magnetic field on free convection flow of nanofluid past a vertical flat plate for four types of nanoparticles. They showed that, although copper and mercury nanoparticles give better cooling performance compared with titanium oxide (TiO_2) and aluminum oxide (Al_2O_3) particles, the advantage is not impressive enough. They also found that the thickness of thermal boundary layer increases with both solid volume fraction of nanofluid and magnetic parameter. Van Gorder *et al*. [10] presented a similarity solution for nano hydrodynamic boundary layer over stretching surfaces. The similarity equations were solved using the homotopy analysis method (HAM). Van Gorder *et al*. [10] found that the surface shear stress decreases as the slip parameter increases. Hamad [11] presented an analytical solution for convection flow of a nanofluid over a stretching plate. A combined similarity numerical solution for convective boundary layer flow of a nanofluid over a vertical plate was obtained by Khan and Aziz [12]. They described the effects of governing parameters on skin friction coefficient, Nusselt number, and Sherwood number. Makinde and Aziz [13] studied the nanofluid boundary layer flow over a linearly stretching sheet with a convective boundary condition. They concluded that the concentration of nanoparticles increases as the convection Biot number increases. Hassani *et al*. [14] applied the HAM to the boundary layer flow of a nanofluid over a horizontal stretching plate. They found that the analytical results for the local Nusselt and Sherwood numbers agree reasonably well with the numerical results presented by Khan and Pop [8]. Rana and Bhargava [15] studied the steady, laminar boundary fluid flow which results from the non-linear stretching of a flat surface in a nanofluid. Some of researchers [16-18] investigated the mono-diffusive and double-diffusive natural convective boundary-layer flow of a nanofluid past a vertical plate. It should be mentioned that Nield and Kuznetsov [19-21], have used in a series of pioneering papers the mathematical nanofluid model proposed by Buongiorno [6] to study some problems on viscous (regular) fluids and porous media filled by nanofluids.

The preceding literature review reveals that the present problem of forced convection boundary layer magnetohydrodynamic (MHD) flow of nanofluid over a permeable stretching plate has remained unexplored. Besides the effects of Brownian motion and thermophoresis, the present work, unlike previous studies, also retains the viscous dissipation term in the energy equation. A similarity analysis is performed to reduce the governing equations to ordinary differential equations which are subsequently solved numerically using an implicit finite difference scheme, popularly known as the Keller-box method. Results presented focus on how the magnetic field, surface mass transfer (suction or injection), viscous dissipation, Brownian motion, and thermophoresis affect the heat and mass transfer characteristics of the flow.

Mathematical formulation

The steady-state 2-D forced convection MHD boundary layer flow of a nanofluid over a permeable horizontal stretching plate is considered, fig. 1. Taking into account the effects of Brownian motion and thermophoresis and based on model developed by Buongiorno [6] the governing equations in the presence of variable magnetic field, and viscous dissipation are as:

$$\frac{\partial u}{\partial x}+\frac{\partial v}{\partial y}=0 \tag{1}$$

$$u\frac{\partial u}{\partial x}+v\frac{\partial u}{\partial y}=\nu\frac{\partial^2 u}{\partial y^2}-\frac{\sigma {B_0}^2}{\rho}u \tag{2}$$

$$u\frac{\partial T}{\partial x}+v\frac{\partial T}{\partial y}=\alpha\nabla^2 T+$$

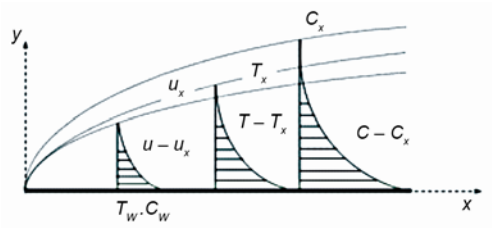

Figure 1. Schematic of the physical model and co-ordinate system

$$+\frac{(\rho C)_P}{(\rho C)_f}\left[D_B\frac{\partial C}{\partial y}\frac{\partial T}{\partial y}+\left(\frac{D_T}{T_\infty}\right)\left(\frac{\partial T}{\partial y}\right)^2\right]+\frac{\mu_f}{(\rho C)_f}\left(\frac{\partial u}{\partial y}\right)^2 \tag{3}$$

$$u\frac{\partial C}{\partial x}+v\frac{\partial C}{\partial y}=D_B\frac{\partial^2 C}{\partial y^2}+\frac{D_T}{T_\infty}\frac{\partial^2 T}{\partial y^2} \tag{4}$$

where the symbols are as defined in the nomenclature.

The second term on the right hand side of eq. 2 represents the effect of magnetic field. In eq. 3, the second term on the right hand side captures the convective transport due to Brownian motion and thermophoresis, while the third term on the right hand side is associated with viscous dissipation. The first and the second terms on the right hand side of eq. 4 represent the diffusion of nanoparticles due to Brownian motion and thermophoresis, respectively.

At the surface of the plate, a no-slip condition is assumed, *i. e.* the velocity along the plate is zero. The component normal to the plate, which is the result of suction or injection at the plate, is assumed to be a function of the co-ordinate x. A constant value for the solid volume fraction of nanofluid at the plate is also assumed. With these assumptions and the standard free stream conditions, the boundary conditions may be written as:

$$v=v_w(x),\quad u_w=ax,\quad T=T_w,\quad C=C_w \text{ at } y=0$$
$$u,v\to 0,\quad T\to T_\infty,\quad C\to C_\infty \text{ as } y\to\infty \tag{5}$$

where the symbols are as defined in the nomenclature.

Following the similarity transformation approach, we introduce the following new variables to transform the governing equations into the ordinary differential equations:

$$\psi=u_w x(\mathrm{Re}_x)^{-0.5}f(\eta),\quad \theta(\eta)=\frac{T-T_\infty}{T_w-T_\infty},\quad \varphi(\eta)=\frac{C-C_\infty}{C_w-C_\infty},\quad \eta=\frac{y}{x}(\mathrm{Re}_x)^{0.5} \tag{6}$$

where the stream function $\psi(x, y)$ is defined as:

$$u=\frac{\partial\psi}{\partial y},\quad v=-\frac{\partial\psi}{\partial x} \tag{7}$$

Using the variables defined by eq. (6), the momentum equation, eq. (2), the energy equation, eq. (3), and the equation for the solid volume fraction of nanofluid, eq. (4) may be rewritten as:

$$f''' + ff'' - (f')^2 - Mnf' = 0 \tag{8}$$

$$\frac{1}{\mathrm{Pr}}\theta'' + f\theta' + Nb\varphi'\theta' + Nt\theta'^2 + \mathrm{Ec}f''^2 = 0 \tag{9}$$

$$\varphi'' + \mathrm{Le}\, f\varphi' + \frac{Nt}{Nb}\theta'' = 0 \tag{10}$$

The original boundary conditions (5) now take the following forms:

$$\begin{aligned} &f(0) = \lambda, \quad f'(0) = 1, \quad \theta(0) = 1, \quad \varphi(0) = 1 \\ &f'(\eta) \to 0, \quad \theta(\eta) \to 0, \quad \varphi(\eta) \to 0 \quad \text{as} \ \ \eta \to \infty \end{aligned} \tag{11}$$

where prime denotes differentiation with respect to η. λ is the suction-injection parameter ($\lambda > 0$ for suction, $\lambda < 0$ for injection) and the dimensionless parameters *Nb, Nt, λ, Mn,* Pr, Le, Re_x, Ec, Nu_x and Sh_x are the Brownian motion parameter, the thermophoresis parameter, the suction-injection parameter, the magnetic parameter, Prandtl, Lewis, Reynolds, Eckert, Nusselt, and Sherwood numbers, respectively. These parameters are defined as follows:

$$\begin{aligned} &Nb = \frac{(\rho C)_P D_B(\varphi_W - \varphi_\infty)}{(\rho C)_f \nu}, \quad Nt = \frac{(\rho C)_P D_T(T_W - T_\infty)}{(\rho C)_f \nu T_\infty}, \quad \lambda = -\nu_w(x)\sqrt{\frac{2x}{\nu u_\infty}}, \quad Mn = \frac{\sigma {B_0}^2 x}{\rho u_\infty}, \\ &\mathrm{Pr} = \frac{\nu}{\alpha}, \quad \mathrm{Le} = \frac{\nu}{D_B}, \quad \mathrm{Re} = \frac{u_w}{\nu}x, \quad Ec = \frac{{u_\infty}^2}{C_f \Delta T}, \quad \mathrm{Nu_x} = -\theta'(0), \quad \mathrm{Sh_x} = -\varphi'(0) \end{aligned} \tag{12}$$

Examining the definitions of suction/injection parameter λ and magnetic parameter *Mn* in eq. 12, it is noted that they are functions of x and not constants as true similarity requires. Because we treat them as constants in the numerical solutions to follow, the results are only locally similar. However, if the magnetic field rate $B_0(x)$ and the velocity $v_w(x)$ are both proportional to $x^{-1/2}$, λ and *Mn* become independent of x, and a true similarity transformation is realized.

Numerical procedure

Equations (8)-(11) are solved numerically using an efficient implicit finite-difference scheme known as the Keller-box method. The method is implemented in four steps. First, eqs. (8)-(10) are reduced to seven first-order differential equations. Second, the equations are discretized using central finite differences. Third, the resulting non-linear algebraic equations are linearized using Newton's method [22-24] and written in matrix vector form. The fourth and final step uses the block-tridiagonal-elimination technique to solve the linearized algebraic equations. A step size of $\Delta\eta = 0.005$ was found to satisfy the convergence criterion of 10^{-4} in all cases. The choice of $\eta_\infty = 6$ satisfactorily covered the entire region of all three boundary layers. The numerical code was validated by comparing the present results with the results in existing literature [8, 25] for the case of boundary layer with no viscous dissipation, no surface mass transfer and no magnetic field ($Mn = \mathrm{Ec} = \lambda = 0$). Also the criterions pointed by Pantokratoras [26] are satisfied. As can be seen from tab. 1 and fig. 2, the comparison shows close agreement between the present results and those available in the literature [8, 25].

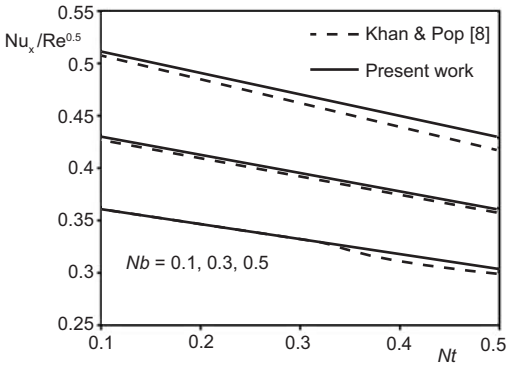

Figure 2(a). Comparison between present results with results obtained by Khan and Pop [8] when Pr =1, Le =10, *Mn* = 0, Ec = 0, and λ = 0

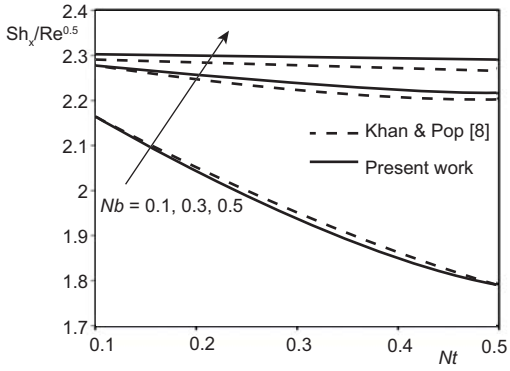

Figure 2(b). Comparison between present results with results obtained by Khan and Pop [8] when Pr =1, Le =10, *Mn* = 0, Ec = 0, and λ = 0

Results and discussion

Table 1. Comparison of present numerical results for reduced Nusselt number $-\theta'(0)$ with results obtained in literature when *Mn* = Ec = λ = 0

Pr	Present results $Nb = Nt = 0$	Wang [25]	Khan and Pop [8]
0.2	0.1695	0.1691	0.1691
0.7	0.4543	0.4539	0.4539
2	0.9112	0.9114	0.9114
7	1.8955	1.8954	1.8954
20	3.3545	3.3539	3.3539
70	6.4721	6.4622	6.4622

The effects of dimensionless governing parameters such as suction-injection parameter, magnetic parameter, Brownian motion parameter, thermophoresis parameter, Prandtl number, Eckert number, and Lewis number on dimensionless velocity, dimensionless temperature, dimensionless nanoparticles fraction, reduced Nusselt, and reduced Sherwood numbers were investigated. Figure 3 represents dimensionless velocity profiles for various values of suction-injection and magnetic field parameters. When fluid is injected normal to the surface of the plate, it tends to push the momentum boundary layer further into the free stream. With suction at the plate, the momentum boundary layer is drawn closer to the surface. Thus compared with the case of no injection (λ = 0), the momentum boundary layer is thicker for injection (λ = –2) and thinner for suction (λ = 2). As the imposed magnetic is increased, it shrinks the boundary layer region. In this respect, the effect of magnetic field is similar to that of suction at the wall. Figures 4 and 5 show that, as thermophoretic effect increases, both the local solid volume fraction of nanofluid and local temperature in the respective boundary layers increase. Although the increase in thermophoresis thicknes the solid volume fraction boundary layer slightly (fig. 4), it has no observable impact on the thickness of thermal boundary layer (fig. 5). As the thermophoresis strengthens *i. e.* for Nt = 0.2 and 0.3, the solid volume fraction curves exhibit peaks with concentrations in the boundary layer exceeding the concentration at the wall (see fig. 4). As can be seen from fig. 5, the thermal boundary layer region shrinks with the increase in Prandtl number, as is the case with a regular fluid. It is interesting to note that the dimensionless temperature in fig. 5 for Nt = 0.1 and 0.15 exceeds unity when Pr = 10. For these two cases, heat transfer is reversed and thermal energy flows from fluid to the wall. The effect of Brownian motion on solid volume fraction of nanofluid is illustrated in fig. 6 in

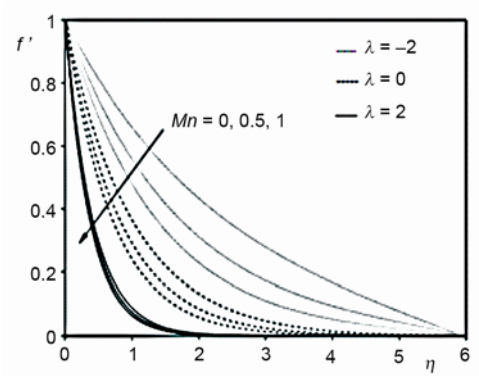

Figure 3. Dimensionless velocity profiles for various values of suction-injection and magnetic field parameter

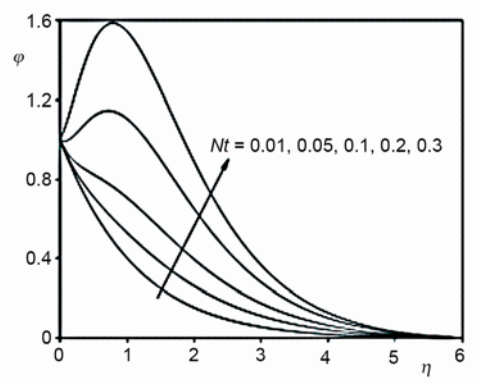

Figure 4. Solid volume fraction of nanofluid profiles for various values of thermophoresis parameter when Pr = 1, Le = 1, *Nb* = 0.1, Ec = 1, and λ = 0.5

presence of the suction-injection parameter. As the Brownian motion intensifies (*Nb* increases), the local solid volume fraction of nanofluid decreases. Also it can be observed that for suction (λ = 0.5) the solid volume fraction boundary layer is thinner compared with the cases for injection (λ = –0.5) and for impermeable surface (λ = 0). In fig. 7, the effect of Brownian motion on dimensionless temperature for various values of suction-injection parameter is presented. As expected, regardless of the value of suction-injection parameter, the local temperature increases with the increase in the Brownian motion parameter. This is due to the increase in the collision of the fluid particles with nanoparticles. Further, for injection (λ = –0.5), the effect of Brownian motion on temperature is more significant. Also this figure compares the dimensionless temperature profile for the impermeable plate (λ = 0) with that for suction (λ = 0.5) and injection (λ = –0.5). This comparison reveals that the boundary layer for the impermeable case (λ = 0) gets heated when the fluid is injected at the plate (λ = –0.5) and gets cooled when suction occurs at the plate (λ = 0.5). Figures 8 and 9 depict the influence of the Eckert number on the distributions of solid volume fraction of nanofluid and dimensionless

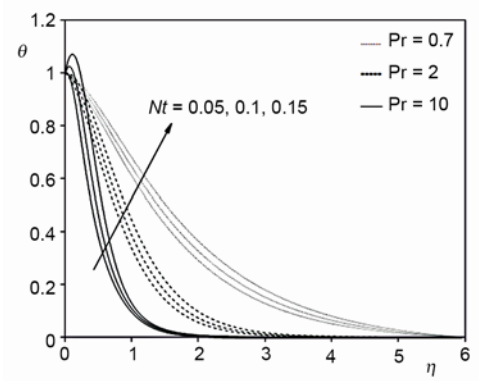

Figure 5. Dimensionless temperature profile as a function of thermophoresis parameter and Prandtl number when Ec = 1, Le = 10, *Mn* = 0.5, *Nb* = 0.1, and λ = 0

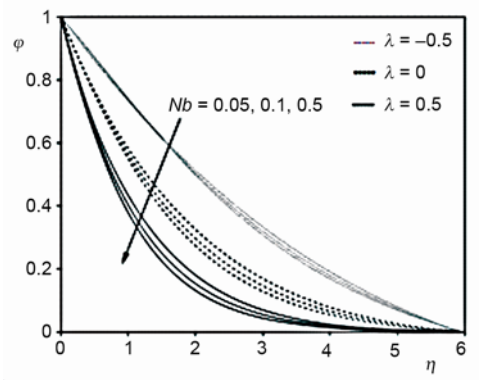

Figure 6. Solid volume fraction of nanofluid *vs.* Brownian motion parameter for various values of suction/injection parameter when Pr = 1, Le = 1, *Nt* = 0.01, *Mn* = 1, and Ec = 1

temperature. While the intensity of viscous dissipation, as measured by the Eckert number strongly influences the temperature distribution (fig. 9), its impact on the solid volume fraction of nanofluid (fig. 8) is relatively weak. Higher temperatures arise due to enhanced internal heat generation associated with increased viscous dissipation. This trend matches with that observed in the boundary layer flow of a regular fluid. Also in fig. 9, it is obvious that local temperature increases with an increase in magnetic field parameter. Figure 10 shows that the effect of Prandtl number on the distribution of solid volume fraction of nanofluid varies within the boundary layer. Near the plate, the solid volume fraction of nanofluid increases as the Prandtl number increases, but the effect is opposite in the region away from the plate (closer to the free stream). Figure 11 illustrates the effect of magnetic field parameter on the distribution of solid volume fraction of nanofluid for different values of Lewis number. It can be seen that the increase in magnetic field parameter, regardless the value of Lewis number, causes an increase in solid volume fraction of nanofluid, but at low values of Lewis number, this effect is more pronounced. Figure 12 shows the reduced Nusselt number as a function of thermophoresis parameter for different values of Eckert number. It is seen that the reduced Nusselt number decreases almost linearly with the thermophoresis parameter. The increase in Eckert

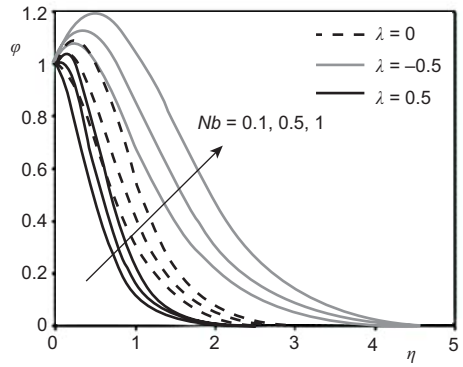

Figure 7. Dimensionless temperature profiles *vs.* Brownian motion parameter for various values of suction/injection parameter when Pr = 3, Le = 3, *Nt* = 0.1, Ec = 1, and *Mn* = 1

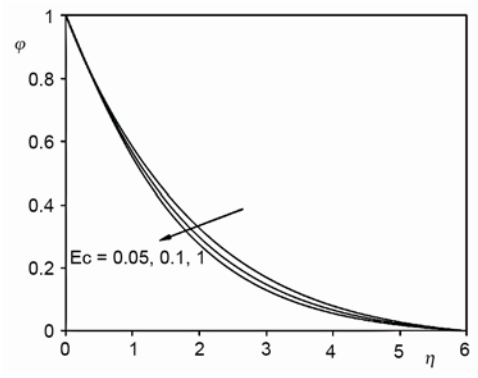

Figure 8. Solid volume fraction of nanofluid for various values of Eckert number when Pr = 1, Le = 1, *Nt* = 0.01, *Nb* = 0.1, *λ* = 0, and *Mn* = 1

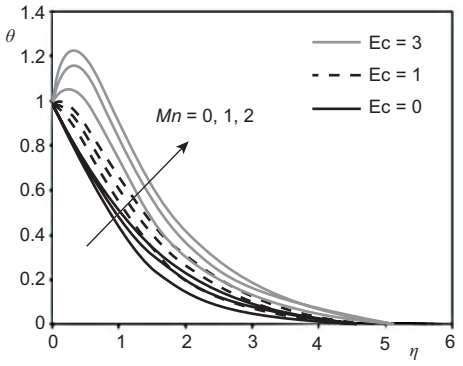

Figure 9. Dimensionless temperature profiles *vs.* magnetic parameter for various values of Eckert number when Pr = 1, Le = 10, *Nt* = 0.1, *Nb* = 0.1, and *λ* = 0

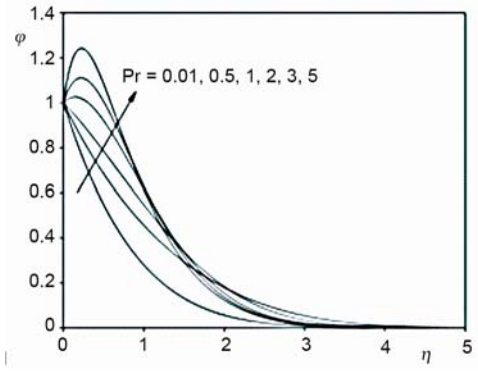

Figure 10. Solid volume fraction of nanofluid for various values of Prandtl number when Ec = 0.5, Le = 3, *Nt* = 0.1, *Nb* = 0.1, *λ* = 1, and *Mn* = 1

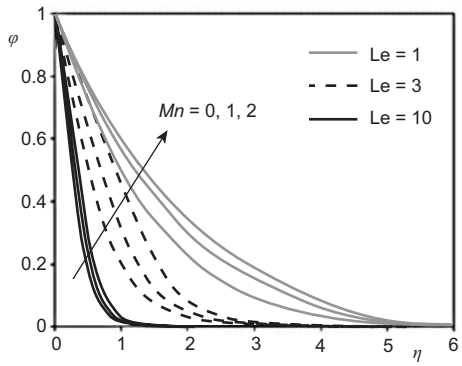

Figure 11. Solid volume fraction of nanofluid for various values of Lewis number and magnetic parameters when Pr = 0.5, Ec = 3, *Nt* = 0.1, and *Nb* = 0.1

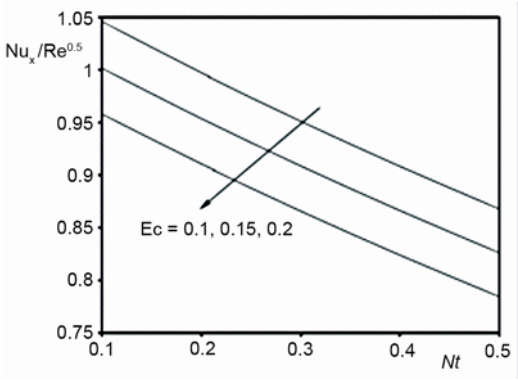

Figure 12. Effects of thermophoresis parameter and Eckert number on reduced Nusselt number when Pr = 1, Le = 10, *Mn* = 1, *Nb* = 0.1, and λ = 0.1

number from 0.1 to 0.2 decreases the reduced Nusselt number. Figure 13 plots the reduced Nusselt number as a function of thermophoresis parameter for parametric values of magnetic field parameter *Mn*. Each of the three curves shows that the reduced Nusselt number decreases as *Mn* increases. Figure 14 shows the reduced Nusselt number as a function of Prandtl number for cases suction (λ = 0.5), injection (λ = –0.5) and impermeable surface (λ = 0). For suction (λ = 0.5), the reduced Nusselt number increases as Prandtl number increases, for impermeable surface (λ = 0), the reduced Nusselt number slightly increases with the increase in Prandtl number and for injection (λ = –0.5) the trend is reversed. Figure 15 plots the reduced Nusselt number as a function of Lewis number Le for parametric values of Brownian motion parameter *Nb*. Each of the three curves shows that the reduced Nusselt number first decreases as Le increases, reaches a minimum, and then increases as Le is further increased. Thus, for certain combination values of *Nb* and Le, the heat transfer from the plate to the flow is minimized. Figure 16 illustrates the reduced Sherwood number (a measure of transport of nanoparticles from the surface into the flow field) as a function of thermophoresis parameter for different values of Eckert number (see also tab. 2). For weak viscous dissipation (Ec = 0.1),

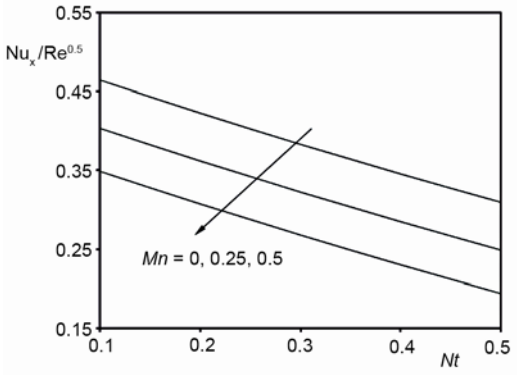

Figure 13. Effects of thermophoresis and magnetic field parameters on reduced Nusselt number when Pr = 1, Ec = 1, Le = 10, *Nb* = 0.1, and λ = 1

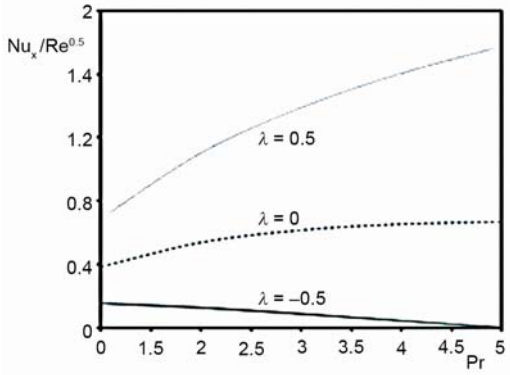

Figure 14. Effects of Prandtl number and suction-injection parameter on reduced Nusselt number when *Nt* = 0.1, Ec = 0.1, Le = 10, *Nb* = 0.1, and *Mn* = 1

Table 2. Reduced Sherwood and reduced Nusselt numbers for various values of governing dimensionless parameters

Nb	*Nt*	Le	Pr	Ec	*Mn*	$\lambda = -0.5$		$\lambda = 0$		$\lambda = 0.5$	
						$-\varphi'(0)$	$-\theta'(0)$	$-\square'(0)$	$-\theta'(0)$	$-\square'(0)$	$-\theta'(0)$
0.1	0.1	10	1	1	0.0	0.3422	–0.0026	2.4234	0.1185	6.1740	0.2800
					0.5	0.3503	–0.1523	2.4618	–0.0297	6.2477	0.1471
					1	0.3643	–0.2775	2.4995	–0.1534	6.3129	0.0353
0.1	0.1	10	1	1	0	0.1698	0.2018	2.0706	0.4473	5.6801	0.7694
					0.5	0.2667	–0.0373	2.2845	0.1477	5.9956	0.4034
					1	0.3643	–0.2775	2.4995	–0.1534	6.3129	0.0353
0.1	0.1	1	1	1	0.1	0.6085	–0.2715	0.4992	–0.1433	0.3030	0.0650
					1	0.6172	–0.2729	0.7763	–0.1520	0.9336	0.0405
					10	0.3643	–0.2775	2.4995	–0.1534	6.3129	0.0353
0.1	0.1	1	10	1	0.1	0.1816	0.1183	2.2471	0.1284	6.1831	0.1386
					1	0.3643	–0.2775	2.4995	–0.1534	6.3129	0.0353
					10	1.2110	–2.3716	4.8998	–2.7766	8.3945	–1.8959
0.1	1	1	10	1	0.1	0.3643	–0.2775	2.4995	–0.1534	6.3129	0.0353
					0.3	0.7771	–0.2937	3.1039	–0.1869	6.7156	–0.0205
					0.5	1.1927	–0.3088	3.7587	–0.2176	7.2582	–0.0717
0.1	1	1	10	1	0.1	0.3643	–0.2775	2.4995	–0.1534	6.3129	0.0353
					0.3	0.2272	–0.2977	2.3170	–0.1787	6.2327	–0.0123
					0.5	0.1997	–0.3142	2.2795	–0.1977	6.2147	–0.0499

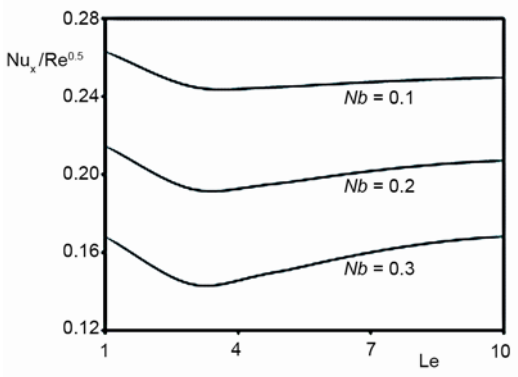

Figure 15. Effects of Lewis number and Brownian motion parameter on reduced Nusselt number when Pr = 1, Ec = 1, *Mn* = 1, *Nt* = 0.1, and λ = 0.1

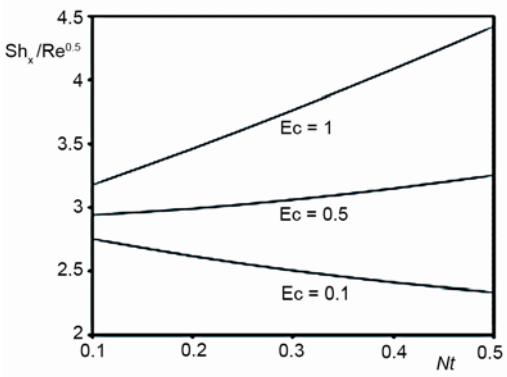

Figure 16. Effects of thermophoresis parameter and Eckert number on reduced Sherwood number when Pr = 1, Le = 10, *Mn* = 1, *Nb* = 0.1, and λ = 1

the reduced Sherwood number decreases as thermophoresis parameter increases, but when viscous dissipation is strong (Ec = 1) the trend is reversed. In Figure 17, we have plotted the reduced Sherwood number as a function of thermophoresis and magnetic field parameters.

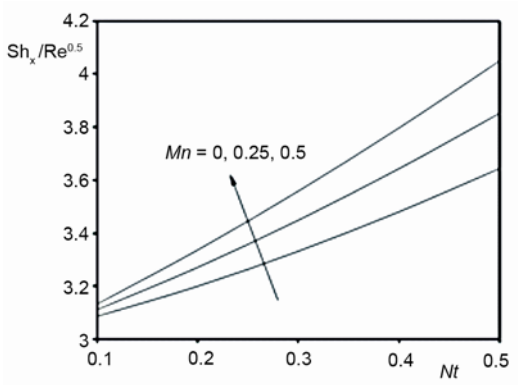

Figure 17. Effects of magnetic field and thermophoresis parameters on reduced Sherwood number when Pr = 1, Le = 10, Ec = 1, *Nb* = 0.1, and λ = 0.1

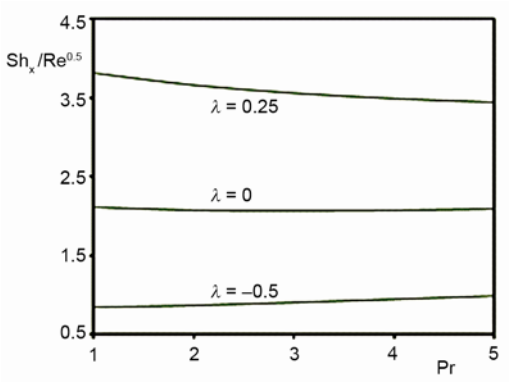

Figure 18. Effects of Prandtl number and suction-injection parameter on reduced Sherwood number when Ec = 0.1, Le = 10, *Nt* = 0.1, *Nb* = 0.1, and *Mn* = 1

The increase in the strength of thermophoresis and/or magnetic field enhances the transport of nanoparticles from the surface into the flow field, as reflected by the increase in the reduced Sherwood number. Figure 18 reveals that for case, λ = 0.25 (suction), while the reduced Sherwood number decreases with the increase in Prandtl number, the trend is reverse for λ = –0.5 (injection) and when λ = 0 (impermeable plate), the reduced Sherwood number is virtually independent of Prandtl number. Figure 19 represents reduced Sherwood number *vs.* Lewis number for different values of Brownian motion parameter. It is seen that the reduced Sherwood number increases almost linearly with the Lewis number. The increase in Brownian motion parameter *Nb* from 0.01 to 0.1 also increases the reduced Sherwood number.

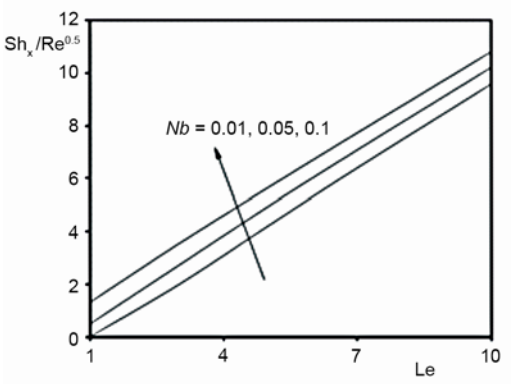

Figure 19. Effects of Lewis number and Brownian motion parameter on reduced Sherwood number when Pr = 1, Ec = 1, *Mn* = 1, *Nt* = 0.1, and λ = 1

Conclusions

Significant conclusions drawn from this study may be summarized as follows.

- The thickness of the boundary layer for the solid volume fraction of nanofluid increases as the thermophoresis effect increases, but the thickness is hardly affected by the changes in Brownian motion and viscous dissipation. At high values of Lewis number, the change in magnetic field has no significant effect on the thickness of boundary layer for the solid volume fraction of nanofluid, but at low values of Lewis number, the solid volume fraction increases slightly with the increase in magnetic field.
- The thickness of the boundary layer for solid volume fraction of nanofluid increases with increasing Brownian effect, but for the case of injection, the Brownian effect on the volume fraction boundary layer thickness is more pronounced than the case of suction.

- The effects of suction/injection parameter, Prandtl number, and Eckert number on thermal boundary layer of a nanofluid is similar to those found in a regular fluid.
- The reduced Sherwood number increases with increasing the magnetic field parameter while when thermophoresis is weak, reduced Sherwood number is hardly affected by changes in magnetic field.
- At low thermophoresis parameter, the reduced Sherwood number is not significantly affected by the increase in Eckert number. Also, the effect of suction-injection parameter on the reduced Nusselt number is more pronounced at high Prandtl numbers.
- For certain combination values of Lewis number and thermophoresis parameter, the reduced Nusselt number attains minimum values, that is, the heat transfer from the plate to the flow is minimized.

Nomenclature

a – constant, [s^{-1}]
B_0 – magnetic field rate, [–]
C – solid volume fraction of nanofluid, [–]
C_w – nanofluid solid volume fraction at the plate, [–]
$(C_p)_f$ – heat capacity of base fluid, [$Jkg^{-1}K^{-1}$]
$(C_p)_p$ – heat capacity of nanoparticles, [$Jkg^{-1}K^{-1}$]
C_∞ – ambient nanofluid solid volume fraction, [–]
D_B – Brownian diffusion coefficient, [m^2s^{-1}]
D_T – thermophoretic diffusion coefficient, [m^2s^{-1}]
Ec – Eckert number, ($= u_\infty^2/C_f\Delta T$), [–]
f – dimensionless stream function, [–]
Le – Lewis number, ($= \nu/D_B$), [–]
Mn – magnetic parameter, ($=\sigma B_0{}^2 x/\rho u_\infty$), [–]
Nb – Brownian motion parameter, $\{=[(\rho C)_P D_B(\varphi_W-\varphi_\infty)]/(\rho C)_f \nu\}$, [–]
Nt – thermophoresis parameter, $[=(\rho C)_P D_T(T_W-T_\infty)/(\rho C)_f \nu T_\infty]$, [–]
Nu_x – Nusselt number, $[=-\theta'(0)]$, [–]
Pr – Prandtl number, ($=\nu/\alpha$), [–]
Re_x – Reynolds number, ($=u_w x/\nu$), [–]
Sh_x – Sherwood number, $[=-\varphi'(0)]$, [–]
T – fluid temperature, [K]
T_w – plate (wall) temperature, [K]
T_∞ – ambient temperature, [K]
u – x component of velocity, [ms^{-1}]
u_w – plate velocity, ($= ax$), [ms^{-1}]
u_∞ – free stream velocity, [ms^{-1}]
v – y component of velocity, [ms^{-1}]
v_w – suction velocity, [ms^{-1}]
x – horizontal co-ordinate, [m]
y – vertical co-ordinate, [m]

Greek symbols

α – thermal diffusivity, ($=k/\rho c$), [m^2s^{-1}]
η – similarity variable, $[=y(Re_x)^{0.5}/x]$, [–]
θ – dimensionless temperature, $(=T-T_\infty/T_w-T_\infty)$, [–]
λ – suction/injection parameter, $[=-v_w(x)\sqrt{2x/\nu u_\infty}]$), [–]
μ_f – dynamic viscosity of base fluid, [Nsm^{-2}]
ν_f – kinematic viscosity of base fluid, [m^2s^{-1}]
ρ_f – density of base fluid, [kgm^{-3}]
ρ_p – density of nanoparticles, [kgm^{-3}]
σ – electric conductivity, [mho s^{-1}]
φ – dimensionless solid volume fraction of nanofluid
ψ – stream function, $[=u_w x(Re_x)^{-0.5}]$, [$m^2\ s^{-1}$]

References

[1] Fisher E. G., *Extrusion of Plastics*, John Wiley and Sons, New York, USA, 1976
[2] Altan, T., Gegel, S. O. H., *Metal Forming Fundamentals and Applications, American Society of Metals*, Metals Park, O., USA, 1979
[3] Tadmor, Z., Klein, I., *Engineering Principles of Plasticating Extrusion,* Polymer Science and Engineering Series, Van Nostrand Reinhold, New York, USA, 1970
[4] Choi, S. U. S., Enhancing Thermal Conductivity of Fluids with Nanoparticles, *Proceedings*, ASME International Mechanical Engineering Congress and Exposition, San Francisco, Cal., USA, ASME, FED 231/MD 66, 1995, pp. 99-105
[5] Choi, S. U. S., *et al*., Anomalously Thermal Conductivity Enhancement in Nanotube Suspensions, *Applied Physics Letters, 79* (2001), 14, pp. 2252-2254
[6] Buongiorno, J., Convective Transport in Nanofluids, *ASME Journal of Heat Transfer*, *128* (2006), 3, pp. 240-250

[7] Bachok, N., *et al*., Boundary-Layer Flow of Nanofluids over a Moving Surface in a Flowing Fluid, *International Journal of Thermal Sciences, 49* (2010), 9, pp. 1663-1668
[8] Khan, W. A., Pop, I., Boundary-Layer Flow of a Nanofluid past a Stretching Sheet, *International Journal of Heat and Mass Transfer, 53* (2010), 11-12, pp. 2477-2483
[9] Hamad, M. A. A., *et al*., Magnetic Field Effects on Free Convection Flow of a Nanofluid past a Vertical Semi-Infinite Flat Plate, *Nonlinear Analysis: Real World Applications, 12* (2011), 3, pp. 1338-1346
[10] Van Gorder, R. A., *et al*., Nano Boundary Layers over Stretching Surfaces. *Communication in Nonlinear Science and Numerical Simulation, 15* (2010), 6, pp. 1494-1500
[11] Hamad, M. A. A., Analytical Solution of Natural Convection Flow of a Nanofluid over a Linearly Stretching Sheet in the Presence of Magnetic Field, *International Communications in Heat and Mass Transfer, 38* (2011), 4, pp. 487-492
[12] Khan, W. A., Aziz, A., Natural Convection Flow of a Nanofluid over a Vertical Plate with Uniform Surface Heat Flux, *International Journal of Thermal Sciences, 50* (2011), 7, pp. 1207-1214
[13] Makinde, O. D., Aziz A., Boundary Layer Flow of a Nanofluid past a Stretching Sheet with a Convective Boundary Condition, *International Journal of Thermal Sciences*, *50* (2011), 7, pp. 1326-1332
[14] Hassani, M., *et al*., An Analytical Solution for Boundary Layer Flow of a Nanofluid past a Stretching Sheet, *International Journal of Thermal Sciences*, *50* (2011), 11, pp. 2256-2263
[15] Rana, P., Bhargava, R., Flow and Heat Transfer of a Nanofluid over a Nonlinearly Stretching Sheet: A Numerical Study, *Communication in Nonlinear Science and Numerical Simulation*, *17* (2012), 1, pp. 212-226
[16] Kuznetsov, A. V., Nield, D. A., Natural Convective Boundary-Layer Flow of a Nanofluid past a Vertical Plate, *International Journal of Thermal Sciences*, *49* (2010), 2, pp. 243-247
[17] Nield, D. A., Kuznetsov, A. V., Double-Diffusive Natural Convective Boundary-Layer Flow of a Nanofluid past a Vertical Plate, *International Journal of Thermal Sciences, 50* (2011), 5, pp. 712-717
[18] Khan, W. A., Aziz, A., Double-Diffusive Natural Convective Boundary Layer Flow in a Porous Medium Saturated with a Nanofluid over a Vertical Plate: Prescribed Surface Heat, Solute and Nanoparticle Fluxes, *International Journal of Thermal Sciences, 50* (2011), 11, pp. 2154-2160
[19] Nield, D. A., Kuznetsov, A. V., Thermal Instability in a Porous Medium Layer Saturated by a Nanofluid, *International Journal of Heat and Mass Transfer*, *52* (2009), 25-26, pp. 5796-5801
[20] Nield, D. A., Kuznetsov, A. V., The Cheng-Minkowycz Problem for the Double-Diffusive Natural Convective Boundary Layer Flow in a Porous Medium Saturated by a Nanofluid, *International Journal of Heat and Mass Transfer*, *54* (2011), 1-3, pp. 374-378
[21] Nield, D. A., Kuznetsov, A. V., The Onset of Convection in a Horizontal Nanofluid Layer of Finite Depth, *European Journal of Mechanics – B/Fluids*, *29* (2010), 3, pp. 217-223
[22] Cebeci, T., Bradshaw, P., *Momentum Transfer in Boundary Layers,* Hemisphere Publishing Corporation, New York, USA, 1977
[23] Cebeci, T., Bradshaw, P., *Physical and Computational Aspects of Convective Heat Transfer,* Springer-Verlag, New York, USA, 1984
[24] Salleh, M. Z., *et al*., Numerical Solutions of the Forced Boundary Layer Flow at a Forward Stagnation Point, *European Journal of Scientific Research, 19* (2008), 1, pp. 644-653
[25] Wang, C. Y., Free Convection on a Vertical Stretching Surface, *Journal of Applied Mathematics and Mechanics* (ZAMM), *69* (1989), 11, pp. 418-420
[26] Pantokratoras, A., A Common Error Made in Investigation of Boundary Layer Flows, *Applied Mathematical Modelling, 33* (2009), 1, pp. 413-422

Paper submitted: April 3, 2012
Paper revised: February 5, 2013
Paper accepted: May 5, 2013